Quantum Information Processing (2019) 18:346
https://doi.org/10.1007/s11128-019-2463-7

Order-encoded quantum image model and parallel histogram specification

Guanlei Xu[1] · Xiaogang Xu[1] · Xun Wang[1] · Xiaotong Wang[2]

Received: 16 April 2019 / Accepted: 25 September 2019 / Published online: 3 October 2019

Abstract
In this paper, the new quantum image representation model OQIM is proposed to provide a representation for digital images on quantum computers in the form of a normalized state. The newly proposed quantum image representation OQIM uses the basis state of a qubit sequence to store the ascending order of each pixel according to their gray values' magnitude for the first time. Then OQIM uses the amplitude probability of a qubit to store the color and uses the amplitude probability of another qubit to store the coordinate position. Based on the OQIM, the mOQIM is proposed as well, which encodes more digital images via one model. Compared with other quantum image models, the OQIM effectively encodes the information of the histogram of the images. Based on the OQIM and the mOQIM, the histogram specification of two images and even the parallel histogram specification at the same time for multiple images are discussed. Experiments and theoretical analysis show that the proposed OQIM quantum image model is more flexible and better suited for histogram specification, histogram equalization and other similar image enhancement method such as luminance correction and so on than the existing models.

Keywords Quantum computation · Image representation · Histogram specification (HS) · Histogram equalization (HE) · Quantum image retrieval and storage

1 Introduction

Since Feynman proposed a novel computation model called as quantum computers [1] in 1982, more and more work and theoretical analysis proved that the quantum computation based on principles of quantum mechanics seems to be much more pow-

✉ Guanlei Xu
xgl_86@163.com

1 College of Computer and Information Engineering, Zhejiang Gongshang University, Hangzhou 310018, China

2 Dalian Navy Academy, Dalian 610018, China

erful than the classical counterparts. Especially after the milestone work by Shor's polynomial time integer factoring [2] and Grover's database fast searching [3], the quantum computation has attracted more and more researchers in various fields such as information theory, cryptography, image processing and so on in computer science [4] because the quantum computation can overcome the problems of the inefficient tasks on classical computers. Therefore, the quantum computation now is considered to be a promising candidate to overcome the limitations of classical computing by more and more researchers [6–20].

Among the various branches in computer science and information science, the image processing [5, 21–28] is an important one and plays a key role in various applications such as multimedia entertainment, satellite sensing, medical imaging and so on. However, with the dramatic development of image sensors, the number of images has become huge and the image size large. As a result, the overwhelming time requirements of classical image processing algorithms cannot afford these tasks. Up till now, there have been multiple quantum image processing applications such as quantum image geometric transform [6–11], quantum image color manipulation [12], quantum image interpolation [17, 18], quantum image matching [19, 20] and so on [13–16, 29–33]. However, there has been no report on the quantum image histogram equalization up till now. Inspired by these existent work [1–20, 29–33] and the advantage of quantum computation, we will discuss the quantum image histogram equalization by making full use of the quantum computation via new quantum image model. Therefore, it is very necessary for us to explore high-performance manners to store and process images for the current various applications.

In this paper, different from the current quantum image models such as [6–18], a novel model (the order-encoded quantum image model: OQIM) is proposed to provide a representation for digital images on quantum computers in normalized states. This new model OQIM captures information of colors, corresponding coordinate positions and the corresponding ascending orders. In addition, OQIM uses the basis state of a qubit sequence to store the ascending order of each pixel according to their gray values' magnitude. OQIM also uses the amplitude probability of a qubit to store the colors like [6] and uses the amplitude probability of another qubit to store the coordinate position of each pixel like [14]. Based on the OQIM for one single image, we also discuss the mOQIM (OQIM for multiple images). Finally, based on the OQIM and the mOQIM, the histogram specification of two images and even the parallel histogram specification at the same time for multiple images are discussed. Since our quantum model makes full use of the order information, some advantages will be exerted fully in some image task such as histogram equalization and so on.

Before discussing our newly proposed model, we first review the related work on the quantum image representation and the corresponding quantum image processing models in Sect. 2. In Sect. 3, the OQIM model will be shown in details from definition, theoretical analysis to preparation and et al. Section 4 shows the OQIM for image histogram specification. Experiments are shown in Sect. 5. Section 6 concludes this paper.

2 Related work

In the last decade, the merging of quantum computation and image processing has proven to be a very fruitful approach to deal with the performance challenges of current image processing applications. At the same time more and more quantum image processing models have been proposed.

Up till now, a great number of research models related to quantum image representation have been involved in this literature, such as the qubit lattice [7], the entangled Image [15], the RealKet [16], the flexible representation for quantum images (FRQI) [6], the multi-channel representation of quantum image (MCRQI) [8], the normal arbitrary quantum superposition state (NASS) [9], the quantum representation for log-polar images [10], the novel enhanced quantum representation (NEQR) [11], the quantum representation for color digital images (NCQI) [12], the quantum representation for infrared images (SQR) [13], the bijective quantum representation (*QSMC & QSNC*) [14], the improved NEQR (INEQR) [17], the generalized quantum image representation (GQIR) [18], etc. These different models have obtained various successful applications in image processing [19, 20].

During these existing quantum image models, FRQI and MCRQI, respectively, process the gray and color images, and their colors are encoded in the amplitude probabilities of one qubit and three qubits [6, 8], respectively. Therefore, the two models' colors need to measure multiple times to retrieve because of the amplitude probabilities. Moreover, *QSMC & QSNC* [14] *employed the* bijective functions to build the model which encoded the colors and the positions via the amplitude probabilities of qubits. It means that the model's both colors and positions need to measure multiple times to retrieve. Different from the above few models, NEQR encoded and stored the colors with the basis state of a qubit sequence like the coordinate positions [14], which is more flexible and better suited for some image processing. In other words, all kinds of models [6–18] have their own advantages and application fields, and the details can be found in the corresponding references [6–18, 29–33].

Inspired by these existing quantum image models [6, 8, 14], combined with our novel idea of magnitude orders suited for certain image processing such as histogram specification and histogram equalization, in this paper, an order-encoded quantum image model (OQIM) is proposed to provide a representation for digital images on quantum computers in the form of a normalized state.

3 Order-encoded quantum image model (OQIM)

In this section, we will first demonstrate the definition and the theoretical expression of OQIM, then the review of the order of the gray values in the classical image, the preparation of OQIM, the storage and retrieval of every pixel including the complexity analysis of every step are explored in great details.

3.1 The theoretical expression

In the classical format, we assume that the image $f(x, y)$ represents the gray value magnitude in the coordinate position (x, y) $(x, y \in \{0, 1, 2, \ldots, 2^n - 1\})$, i.e., the image has 2^n X-coordinates and 2^n Y-coordinates, respectively. At the same time, the gray value of this image is assumed to be in $[0, L]$ (e.g., $L = 255$). Therefore, if we sort these pixels according to their gray value magnitude in ascending order, this sorted order has 2^{2n} elements (0, 1, 2,…,$2^{2n}-1$, which will be used in the following section of this paper).

Now let's see the definition of OQIM first.

Definition 1 For a given classical image $f(x, y)$ with 2^n X-coordinates and 2^n Y-coordinates, its order-encoded quantum image model (OQIM) is defined by the following expression:

$$|I\rangle = \frac{1}{2^{n+1/2}} \sum_{i=0}^{2^{2n}-1} |cp_i\rangle \otimes |i\rangle, \tag{1}$$

where $|cp_i\rangle = \cos\theta_i|00\rangle + \sin\theta_i|10\rangle + \cos\varphi_i|01\rangle + \sin\varphi_i|11\rangle$ represents both the coordinate and color (the superposition of $|00\rangle, |10\rangle, |01\rangle, |11\rangle$ with the probability amplitudes $\cos\theta_i, \sin\theta_i, \cos\varphi_i, \sin\varphi_i$, respectively); $|i\rangle$ encodes the sorted position with the basis state of a qubit sequence (the superposition of $|o_{i,2n-1}o_{i,2n-2}\cdots o_{i,1}o_{i,0}\rangle (\in \mathrm{B}^{2n}$, which is the $2n$−D Boolean space) from $|00\cdots00\rangle$ to $|11\cdots11\rangle$). "$\otimes$" denotes the tensor product operator.

In Eq. (1), $\cos\theta_i|00\rangle + \sin\theta_i|10\rangle$ represents the color quantum state (which encodes the gray value θ_i which is mapped to $[0, \pi/2]$ from the scope $[0, L]$, L is the max gray level, e.g., 255) of image in pixel i, and $|0\rangle, |1\rangle$ are the base states, $\theta = (\theta_0, \theta_1, \ldots \theta_{2^{2n}-1})$ is the angle vector with $\theta_i \in [0, \pi/2]$.

On the other hand, $\cos\varphi_i|01\rangle + \sin\varphi_i|11\rangle$ represents the ith coordinate quantum state according to the real coordinate position in the image with $\varphi = (\varphi_0, \varphi_1, \ldots \varphi_{2^{2n}-1})$ being the angle vector. In the same manner, φ_i is mapped to $[0, \pi/2]$ from the scope $\left[0, 2^{2n} - 1\right]$. The detailed example of the real coordinate positions in the image is shown in Fig. 1.

We note that the qubit ρ control the distinguishability between the color and the coordinate position. When $|p\rangle = |1\rangle$, it means that we represent the coordinates by $|cp_i\rangle$. When $|p\rangle = |0\rangle$, it means that we represent the colors by $|cp_i\rangle$.

Specially, in Eq. (1), $|i\rangle$ is called as sorted position, i.e.,

$$|i\rangle = |O_i\rangle = |o_{2n-1}o_{2n-2}\cdots o_1o_0\rangle = \left\{ \left|\underbrace{00\cdots00}_{2n}\right\rangle, \left|\underbrace{00\cdots01}_{2n}\right\rangle, \ldots, \left|\underbrace{11\cdots11}_{2n}\right\rangle \right\}, \tag{2}$$

which is the 2^{2n}–D quantum base state, i.e., $i = 0, 1, 2, \ldots, 2^{2n} - 1$ in sorted order, which accords to the ascending sorted order of every pixels' gray value in the image, i.e.,

Fig. 1 The real coordinate position (encoded in the state $|pc\rangle$) in the square image

0	1	2	……	2^n-1
2^n	2^n+1	2^n+2	……	2^{n+1}-1
⋮	⋮	⋮	……	⋮
2^{2n-1}	2^{2n-1}+1	2^{2n-1}+2	……	2^{2n}-1

Fig. 2 The circuit of OQIM for a quantum image

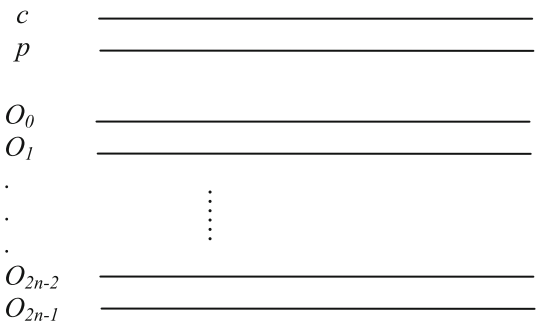

$$\theta_i \le \theta_j \text{ if } \quad i < j\Big(i, j \in \Big\{0, 1, \cdots, 2^{2n} - 1\Big\}\Big).$$

Note that in our model OQIM, there are two positions, one is the sorted position and the other one is the real coordinate position. The sorted position is encoded by $|i\rangle$, and the real coordinate position is encoded by $|pc_i\rangle$ combined with the corresponding gray value.

In Fig. 2, the circuit of OQIM for a quantum image is shown, and we find that for a given image with the size of $2^n \times 2^n$, we need $(2n + 2)$ qubits to encode (or store) it.

Clearly, at the same time, we also have

$$\| |I\rangle \| = \frac{1}{2^{n+1/2}} \left[\sum_{i=0}^{2^{2n}-1} \left(\cos^2 \theta_i + \sin^2 \theta_i + \cos^2 \varphi_i + \sin^2 \varphi_i \right) \right]^{\frac{1}{2}} = 1. \qquad (3)$$

It means that our quantum image model OQIM is unitary according to Eq. (3).

Figure 3 is an example of one 2×2 sized OQIM image ($n = 1$), and Eq. (4) is the corresponding mathematical expression of the corresponding OQIM image. It is clearly shown that the sorted position information is encoded by $|o_1 o_0\rangle$, and the

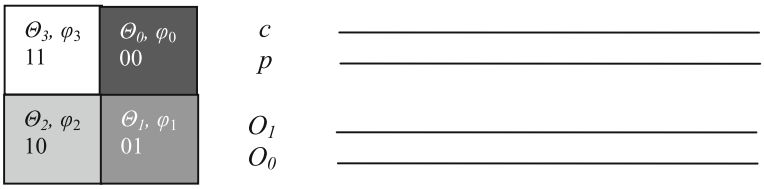

Fig. 3 An example of one 2×2 sized OQIM image ($n = 1$)

information of the gray values and the real coordinate positions is encoded by $|cp\rangle$. See details in Eq. (4).

$$
\begin{aligned}
|I\rangle = \frac{1}{2^{3/2}}[&(\cos\theta_0|00\rangle + \sin\theta_0|10\rangle + \cos\varphi_0|01\rangle + \sin\varphi_0|11\rangle) \otimes |00\rangle \\
&+ (\cos\theta_1|00\rangle + \sin\theta_1|10\rangle + \cos\varphi_1|01\rangle + \sin\varphi_1|11\rangle) \otimes |01\rangle \\
&+ (\cos\theta_2|00\rangle + \sin\theta_2|10\rangle + \cos\varphi_2|01\rangle + \sin\varphi_2|11\rangle) \otimes |10\rangle \\
&+ (\cos\theta_3|00\rangle + \sin\theta_3|10\rangle + \cos\varphi_3|01\rangle + \sin\varphi_3|11\rangle) \otimes |11\rangle]
\end{aligned} \quad . \tag{4}
$$

At the same time in Eq. (4) we also have $\theta_0 < \theta_1 < \theta_2 < \theta_3$ that encodes the colors (gray value magnitudes). $\varphi_{i=0,1,2,3}$ ($\varphi_0 \leftrightarrow 1$, $\varphi_1 \leftrightarrow 3$, $\varphi_2 \leftrightarrow 2$, $\varphi_3 \leftrightarrow 0$) are the real coordinate positions (mapped from $\left[0, 2^{2n} - 1\right]$) of the image in the format of Fig. 1.

3.2 The preparation of OQIM

In quantum computation, the preparation process can transform from an initialized quantum state to the desired quantum image state required for further processing. This transformation involves unitary transforms described by unitary matrices. The preparation process of OQIM will involve some unitary transforms described by unitary matrices in the next sections, and at the same time the preparation theorem PPT [6] and the polynomial preparation theorem PPT [8] guarantee the success of the preparation of OQIM.

3.2.1 The order of the gray values in the classical image

In order to map the classical images to the OQIM images, before the preparation of OQIM, we must sort the classical image according to the gray value magnitudes. In classical computer, this step can be performed easily by the following algorithm.

Algorithm I (Sorting the classical image):

1. ***Initialization:*** $S_{order}[i,j]=[\ ]_{2\times 2^{2n}}$ *is a* 2×2^{2n} *sized array (*$i=1,2;\ j=1,2,\cdots,2^{2n}$*) used to store the two parameters (color and coordinate, respectively),* $S_{temp}[k_1,k_2]=[\ ]_{3\times L}$ *is a* $3\times L$ *sized cell (*$k_1=1,2,3;k_2=1,2,\cdots,L$*) used to dynamically store the sorted orders temporarily; Here we assume* $f(x,y)$ *lies in the gray value scope* $[0,L]$ *that are discrete integers;*

2. ***For*** $(x,y)=(0,0)$ *to* $(2^n-1,2^n-1)$ ***do***

$S_{temp}=[1,f(x,y)]+1\rightarrow S_{temp}[1,f(x,y)]$, *which denotes counting the number of every gray level form 0 to L;*

$\{S_{temp}(2,f(x,y));f(x,y)\}\rightarrow S_{temp}[2,f(x,y)]$, *which denotes storing the colors;*

$\{S_{temp}[3,f(x,y)];(x,y)\}\rightarrow S_{temp}[3,f(x,y)]$, *which denotes storing the coordinates;*

3. ***For*** $l=0$ *to* L ***do***

For $m=1$ *to* $S_{temp}(1,l)$ ***do***

$S_{temp}[2,l](m)\rightarrow S_{order}(1,sum(S_{temp}[1,0:l-1])+m)$,

$S_{temp}[3,l](m)\rightarrow S_{order}(2,sum(S_{temp}[1,0:l-1])+m)$.

In Algorithm I, $S_{\text{temp}}(\cdot,l)(m)$ denotes the m'th element in $S_{\text{temp}}[\cdot,l]$; sum($S_{\text{temp}}[1,0:l-1]$) performs the sum of all the elements from $S_{\text{temp}}[1,0]$ to $S_{\text{temp}}[1,l-1]$. After performing Algorithm I, we can obtain the sorted image, in which the indexes are the sorted positions, and every index points to its two parameters: color and coordinate. That is to say, through the sorted positions, we can retrieve every pixel including its gray value and the corresponding real coordinate.

The above processing is performed in the classical computer before the preparation of OQIM. We find that the complexity of our Algorithm I is about $O(n)$ (here n is the total number of the data to be sorted), which is much less than other sorting method such as bubble sorting with the complexity $O(n^2)$. In addition, in our algorithm there is no comparison operation and most of our operations are assignments of values.

3.2.2 The preparation of OQIM

How to prepare OQIM from quantum computer will be discussed in this section.

Firstly, for a 2^{2n} sorted positions and two qubits for color and coordinate of an image, a quantum register with $2n+2$ qubits needs to be initialized by the following equation:

$$|I\rangle_{in}=|0\rangle^{\otimes 2n+2}. \tag{5}$$

At the same time, we have two common single quantum gates I (Identity matrix) and H (Hadamard matrix) are shown in the following Eq. (6), which will be utilized to build the important quantum operator U_1.

$$I = \begin{bmatrix} 1 & 0 \\ 0 & 1 \end{bmatrix}, \quad H = \frac{1}{\sqrt{2}} \begin{bmatrix} 1 & 1 \\ 1 & -1 \end{bmatrix} \quad U_1 = I \otimes H^{\otimes 2n+1}. \tag{6}$$

Then, the following Eq. (7) is employed to represent quantum transformation from the initial state $|I\rangle_{in}$ to the middle state $|I\rangle_{mi}$ via using the quantum operator U_1.

$$\begin{aligned} |I\rangle_{mi} &= U_1(|I\rangle_{in}) = I \otimes H^{\otimes 2n+1}\left(|0\rangle^{\otimes 2n+2}\right) \\ &= I(|0\rangle) \otimes H(|0\rangle) \otimes H^{\otimes 2n}\left(|0\rangle^{\otimes 2n}\right) \\ &= \frac{1}{2^{n+1/2}}|0\rangle \otimes \sum_{l=0}^{1} |l\rangle \otimes \sum_{i=0}^{2^{2n}-1} |i\rangle. \end{aligned} \tag{7}$$

In fact, at the current time the middle state $|I\rangle_{mi}$ is a null quantum state with 2^{2n} sorted positions because of the lack of colors and coordinates. That is to say, now every sorted position is stored into a normalized quantum superposition state, and at the same time both the color value and coordinate are always 0 (i.e., the corresponding gray value is always 0, and the coordinate is always 0 for every pixel after reverse mapping because $\cos 0|0\rangle + \sin 0|1\rangle = |0\rangle$). Therefore, in the following step we must perform the next quantum transformation to assign the color values and coordinates to these sorted positions by the superposed 2^{2n} quantum states.

Considering the rotation matrices (the rotations about Y axis by the angle 2θ and 2φ, respectively),

$$R_y(2\theta) = \begin{bmatrix} \cos\theta & -\sin\theta \\ \sin\theta & \cos\theta \end{bmatrix} \quad \text{and} \quad R_y(2\varphi) = \begin{bmatrix} \cos\varphi & -\sin\varphi \\ \sin\varphi & \cos\varphi \end{bmatrix}, \tag{8}$$

we can construct two control rotation matrices for the color values and coordinates, respectively,

$$\begin{aligned} R_{c,i} &= R_y(2\theta_i) \otimes (|0\rangle\langle 0|) \\ R_{p,i} &= R_y(2\varphi_i) \otimes (|1\rangle\langle 1|). \end{aligned} \tag{9}$$

Then we can obtain the quantum transformation operator $R_i = R_{c,i} R_{p,i}$ and $R_{cp,i}$ with $i = 0, 1, \cdots, 2^{2n} - 1$ based on Eq. (9),

$$R_{cp,i} = \left(I^{\otimes 2} \otimes \sum_{j=0, j\neq i}^{2^{2n}-1} |j\rangle\langle j| \right) + R_i \otimes |i\rangle\langle i|. \tag{10}$$

In addition, we also have $R_{cp,i} R_{cp,i}^{\dagger} = I^{\otimes 2n+2}$ ("†" denotes the conjugate transpose operator), which means that the quantum transformation operator $R_{cp,i}$ is a unitary

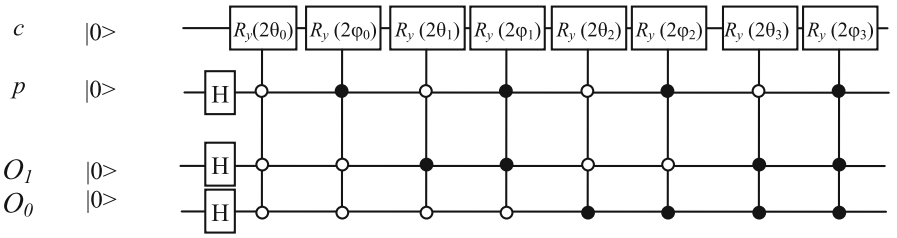

Fig. 4 A simple example of the preparation circuit for the OQIM of the quantum image shown in Fig. 3

matrix. Furthermore, applying the quantum transformation operator $R_{cp,i}$ (let $i = k$) on $|I\rangle_{mi}$ gives us the following relation:

$$\begin{aligned} R_{cp,k}(|I\rangle_{mi}) &= R_{cp,k}\left(\frac{1}{2^{n+1/2}}|0\rangle \otimes \sum_{l=0}^{1}|l\rangle \otimes \sum_{i=0}^{2^{2n}-1}|i\rangle\right) \\ &= \left(I^{\otimes 2} \otimes \sum_{j=0,j\neq k}^{2^{2n}-1}|j\rangle\langle j| + R_k \otimes |k\rangle\langle k|\right)\left(\frac{1}{2^{n+1/2}}|0\rangle \otimes \sum_{l=0}^{1}|l\rangle \otimes \sum_{i=0}^{2^{2n}-1}|i\rangle\right) \\ &= \frac{1}{2^{n+1/2}}\left((\cos\theta_k|00\rangle + \sin\theta_k|10\rangle + \cos\varphi_k|01\rangle + \sin\varphi_k|11\rangle) \otimes |k\rangle + |0\rangle \otimes \sum_{l=0}^{1}|l\rangle \otimes \sum_{i=0,i\neq k}^{2^{2n}-1}|i\rangle\right). \end{aligned} \tag{11}$$

Now we can let $R_{cp} = R_{cp,0}R_{cp,1}\cdots R_{cp,2^{2n}-1}$ and perform R_{cp} on $|I\rangle_{mi}$ to get the final preparation of OQIM as shown in Eq. (12), which is firstly defined in Definition 1.

$$\begin{aligned} R_{cp}(|I\rangle_{mi}) &= R_{cp}\left(\frac{1}{2^{n+1/2}}|0\rangle \otimes \sum_{l=0}^{1}|l\rangle \otimes \sum_{i=0}^{2^{2n}-1}|i\rangle\right) \\ &= \frac{1}{2^{n+1/2}}\sum_{i=0}^{2^{2n}-1}(\cos\theta_i|00\rangle + \sin\theta_i|10\rangle + \cos\varphi_i|01\rangle + \sin\varphi_i|11\rangle) \otimes |i\rangle. \end{aligned} \tag{12}$$

We easily find that the complexity of this preparation of OQIM is about $O\left(2^{4n}\right)$, which is similar with [6].

Figure 4 is a simple example of the preparation circuit for the OQIM of a quantum image with $n = 1$, in which there are some simple quantum gates such as the Hadamard gate (H gate) and 3-qubit control rotation gate used to prepare the OQIM.

3.2.3 Quantum compression in the preparation of OQIM

As shown in [6], quantum image compression is the procedure that reduces the quantum resources used to prepare or reconstruct quantum images. In other words, the main resource in quantum computation is the number of simple quantum gates or simple operations used in the computation. Therefore, in [6] the quantum image compression (QIC) is defined as the process decreasing the number of simple quantum gates in

the preparation and reconstruction of quantum images. On the other hand, since the preparation and reconstruction of quantum images are the same in the sense of their computation, it is sufficient that only the preparation is considered carefully.

For the gray values (or colors) encoded in $\theta_i (i = 0, 1, \ldots, 2^{2n}-1)$, in the same manner as that in [6], taking into account of the fact that the classical image representations use a limited number of levels for expressing gray scales or colors in digital images with various sizes without significant impact on the quality of the images, we can encode the input angles of colors from a discrete set of numbers. Consequently, in the preparation process, controlled rotation operators with the same angle but different conditions affect the positions having the same colors. Therefore, all rotations can be divided into groups such that each group includes only operators having the same rotation angle. This compression procedure is the same as that of [6]. On the other hand, the coordinate positions encoded by $\varphi_i (i = 0, 1, \ldots, 2^{2n} - 1)$ have different values for every pixel; therefore, it is hard to perform the similar quantum image compression operation on φ_i.

4 OQIM for image histogram specification

Histogram specification (HS) [5, 21, 24] is an important image processing technique that is a basic histogram modeling technique that transforms one histogram into another one by remapping the pixel values to manipulate the relative frequency of their occurrence. Up till now, HS has been used for various applications such as image enhancement [21–24], illumination normalization [25, 26], etc., to yield better image quality. In this paper, we will discuss one rather straightforward HS method based on sorting the pixels by the intensities only for quantum images as shown in the following algorithm.

Algorithm II (histogram specification for two images):

1. ***Initialization:*** *Assume* $S^1_{order}[i, j]$ *and* $S^2_{order}[i, j]$ *are the two arrays of size* 2×2^{2n} *for the two images* $f_1(x, y)$ *and* $f_2(x, y)$*, respectively, which are computed from* ***Algorithm I****;*
2. ***For*** $l = 0$ *to* $2^{2n}-1$ ***do***

   $S^1_{order}[1, l] \leftrightarrow S^2_{order}[1, l]$ *("*$\leftrightarrow$*"denotes the swap operator);*
3. ***Reconstruct*** *the two images by*

$$S^1_{order}[1:2, l] \Rightarrow f_1(x, y)$$
$$S^2_{order}[1:2, l] \Rightarrow f_2(x, y).$$

Clearly, in Algorithm II we exchange the corresponding gray values according to the sorted orders, i.e., transform the histogram of $f_1(x, y)$ into $f_2(x, y)$ and transform the histogram of $f_2(x, y)$ into $f_1(x, y)$. Thus, we obtained the histogram specification of one another for the two images.

Now in the following section, we will first give the OQIM for multiple images.

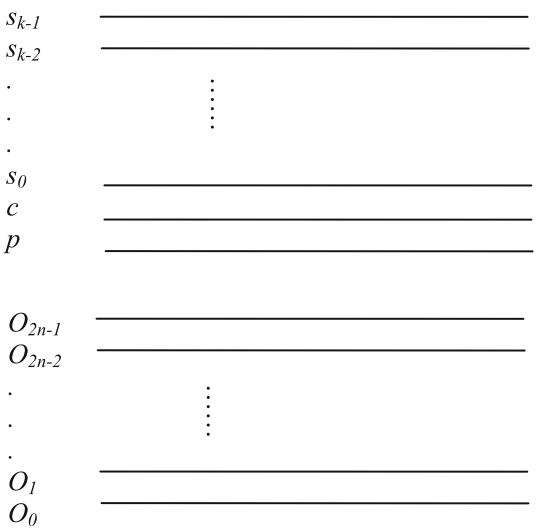

Fig. 5 The circuit of OQIM for $m = 2^k$ quantum images

4.1 mOQIM

Now let's see the definition of OQIM for multiple images (*mOQIM*) first.

Definition 2 For $m = 2^k$ classical image $f_j(x, y)(j = 0, 1, 2, \ldots, m-1)$, their order-encoded quantum image model (called as mOQIM) is defined as follows:

$$\left|I^{(m)}\right\rangle = \frac{1}{2^{k/2}} \sum_{j=0}^{2^k-1} |j\rangle \otimes \left|I_j\right\rangle, \tag{13}$$

where

$$|j\rangle = |s_{k-1}s_{k-2}\cdots s_1 s_0\rangle = \left\{ \left|\underbrace{00\cdots00}_{k}\right\rangle, \left|\underbrace{00\cdots01}_{k}\right\rangle, \cdots, \left|\underbrace{11\cdots11}_{k}\right\rangle \right\},$$

$$\left|I_j\right\rangle = \frac{1}{2^{n+1/2}} \sum_{i=0}^{2^{2n}-1} \left|cp_{j,i}\right\rangle \otimes |i\rangle$$

$$= \frac{1}{2^{n+1/2}} \sum_{i=0}^{2^{2n}-1} \left(\cos\theta_{j,i}|00\rangle + \sin\theta_{j,i}|10\rangle + \cos\varphi_{j,i}|01\rangle + \sin\varphi_{j,i}|11\rangle\right) \otimes |i\rangle$$

In fact, if $m = 2^k = 2^0 = 1$, Definition 2 reduces to Definition 1. At the same time, $\left|I^{(m)}\right\rangle$ is also unitary.

In Fig. 5, the circuit of mOQIM for multiple ($m = 2^k$) quantum images is shown, and we find that for the given images with the size of $2^n \times 2^n$, we need $(2n + k + 2)$ qubits to encode (or store) them.

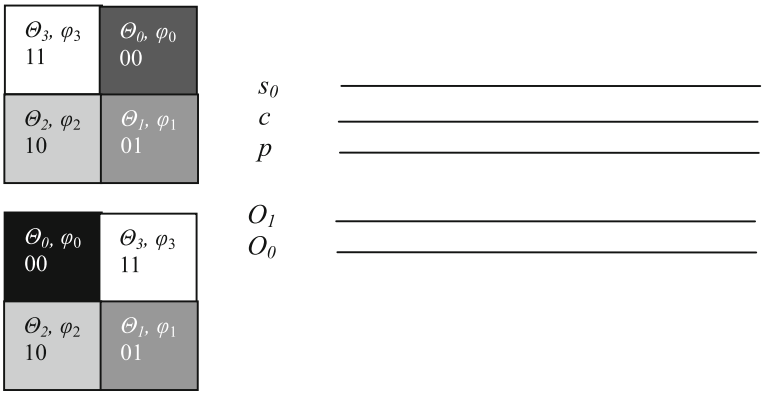

Fig. 6 An example of two 2×2 sized mOQIM images ($n = 1, k = 1, m = 2$)

Figure 6 is an example of the 2×2 sized mOQIM images ($n = 1, k = 1, m = 2$), and Eq. (14) is the corresponding mathematical expression of the corresponding mOQIM images. It is clearly shown that the sorted position information is encoded by $|o_1 o_0\rangle$, and the information of the gray values and the real coordinate positions is encoded by $|cp\rangle$. See details in Eq. (14). $|s_0\rangle$ is used to distinguish/encode the two images $|I_0\rangle$ and $|I_1\rangle$.

$$\left|I^{(2)}\right\rangle = \frac{1}{2^{1/2}} \sum_{j=0}^{1} |I_j\rangle \otimes |j\rangle = \frac{1}{\sqrt{2}} (|I_0\rangle \otimes |0\rangle + |I_1\rangle \otimes |1\rangle), \tag{14}$$

where

$$\begin{aligned} |I_0\rangle = \frac{1}{2^{3/2}} \big[& \big(\cos\theta_{0,0}|00\rangle + \sin\theta_{0,0}|10\rangle + \cos\varphi_{0,0}|01\rangle + \sin\varphi_{0,0}|11\rangle\big) \otimes |00\rangle \\ & + \big(\cos\theta_{0,1}|00\rangle + \sin\theta_{0,1}|10\rangle + \cos\varphi_{0,1}|01\rangle + \sin\varphi_{0,1}|11\rangle\big) \otimes |01\rangle \\ & + \big(\cos\theta_{0,2}|00\rangle + \sin\theta_{0,2}|10\rangle + \cos\varphi_{0,2}|01\rangle + \sin\varphi_{0,2}|11\rangle\big) \otimes |10\rangle \\ & + \big(\cos\theta_{0,3}|00\rangle + \sin\theta_{0,3}|10\rangle + \cos\varphi_{0,3}|01\rangle + \sin\varphi_{0,3}|11\rangle\big) \otimes |11\rangle \big], \end{aligned}$$

$$\begin{aligned} |I_1\rangle = \frac{1}{2^{3/2}} \big[& \big(\cos\theta_{1,0}|00\rangle + \sin\theta_{1,0}|10\rangle + \cos\varphi_{1,0}|01\rangle + \sin\varphi_{1,0}|11\rangle\big) \otimes |00\rangle \\ & + \big(\cos\theta_{1,1}|00\rangle + \sin\theta_{1,1}|10\rangle + \cos\varphi_{1,1}|01\rangle + \sin\varphi_{1,1}|11\rangle\big) \otimes |01\rangle \\ & + \big(\cos\theta_{1,2}|00\rangle + \sin\theta_{1,2}|10\rangle + \cos\varphi_{1,2}|01\rangle + \sin\varphi_{1,2}|11\rangle\big) \otimes |10\rangle \\ & + \big(\cos\theta_{1,3}|00\rangle + \sin\theta_{1,3}|10\rangle + \cos\varphi_{1,3}|01\rangle + \sin\varphi_{1,3}|11\rangle\big) \otimes |11\rangle \big]. \end{aligned}$$

In Fig. 6, if we want to retrieve some pixel's value (e.g., the second image's second pixel's value which was encoded by the quantum state $|10011\rangle$), we only need to

perform the following projection operator $P_1 = |10011\rangle\langle 10011|$ (which belongs to the Hilbert Space) on $|I_2\rangle$ by

$$\theta_{1,1} = \arcsin\left(\frac{\sqrt{P_1\left(\left|I^{(2)}\right\rangle\right)}}{\frac{1}{2^{3/2}}}\right). \tag{15}$$

In the same manner, if we want to retrieve some pixel's real position or coordinate (e.g., the second image's second pixel's coordinate which was encoded by the state $|11011\rangle$) in Fig. 6, we also only need to perform such projection operator $P_2 = |11011\rangle\langle 11011|$ (which belongs to the Hilbert Space) on $|I_2\rangle$ by

$$\varphi_{1,1} = \arcsin\left(\frac{\sqrt{P_2\left(\left|I^{(2)}\right\rangle\right)}}{\frac{1}{2^{3/2}}}\right). \tag{16}$$

In fact, since $\theta_{1,1}$ and $\varphi_{1,1}$ are encoded in the amplitude probability $\frac{1}{2^{3/2}}\sin\theta_{1,1}$ and $\frac{1}{2^{3/2}}\sin\varphi_{1,1}$, respectively (i.e., $\Pr(|10011\rangle) = \frac{1}{2^3}\sin^2\theta_{1,1}$, $\Pr(|11011\rangle) = \frac{1}{2^3}\sin^2\varphi_{1,1}$), they cannot be determined directly by the above two expressions (15) and (16). Only after multiple times' measurements, we can obtain the two values $\theta_{1,1}$ and $\varphi_{1,1}$ by

$$\theta_{1,1} = \arcsin\sqrt{2^3 \cdot Pr(|10011\rangle)} \quad \text{and} \quad \varphi_{1,1} = \arcsin\sqrt{2^3 \cdot Pr(|11011\rangle)}. \tag{17}$$

Then we can remap $\theta_{1,1}$ and $\varphi_{1,1}$ to the scopes $[0, L]$ and $\left[0, 2^{2n}-1\right]$ to get the gray value and the XY coordinate. Thus, in this manner, we can retrieve any pixel's gray value and coordinate in any image from mOQIM. Therefore, we must prepare multiple versions for multiple measurements.

Note that here we use the following projection relation with $P = |k\rangle\langle k|$ and $|I\rangle = \frac{1}{2^{n/2}}\sum_{i=0}^{2^n-1}|i\rangle$

$$P|I\rangle = |k\rangle\langle k|\frac{1}{2^{n/2}}\sum_{i=0}^{2^n-1}|i\rangle = \frac{1}{2^{n/2}}\sum_{i=0}^{2^n-1}|k\rangle\langle k||i\rangle$$
$$= \frac{1}{2^{n/2}}\left(\sum_{i=0,i\neq k}^{2^n-1}|k\rangle\langle k||i\rangle + |k\rangle\langle k||k\rangle\right) = \frac{|k\rangle}{2^{n/2}} \quad \text{because} \quad |k\rangle\langle k||i\rangle = 0 \text{ for } k \neq i.$$

4.2 The preparation of mOQIM

Firstly, for the 2^{2n} sorted positions and 2 qubits for color and coordinate of m images, a quantum register with $2n + k + 2$ qubits needs to be initialized by the following equation:

$$\left|I^{(m)}\right\rangle_{in} = |0\rangle^{\otimes 2n+k+2}. \tag{18}$$

At the same time, based on the two common single quantum gates I and H shown in Eq. (6), which will be utilized to build the important quantum operator U_1.

$$U_1 = H^{\otimes k+1} \otimes I \otimes H^{\otimes 2n}. \tag{19}$$

Then, the following Eq. (20) is employed to represent quantum transformation from the initial state $\left|I^{(m)}\right\rangle_{in}$ to the middle state $\left|I^{(m)}\right\rangle_{mi}$ via using the quantum transformation operator U_1.

$$\begin{aligned}\left|I^{(m)}\right\rangle_{mi} &= U_1\left(\left|I^{(m)}\right\rangle_{in}\right) = H^{\otimes k+1} \otimes I \otimes H^{\otimes 2n}\left(|0\rangle^{\otimes 2n+k+2}\right) \\ &= H^{\otimes k+1}\left(|0\rangle^{\otimes k+1}\right) \otimes I(|0\rangle) \otimes H^{\otimes 2n}\left(|0\rangle^{\otimes 2n}\right) \\ &= \frac{1}{2^{n+\frac{k+1}{2}}} \sum_{j=0}^{2^k-1} |j\rangle \otimes \left(\sum_{l=0}^{1} |l\rangle \otimes |0\rangle\right) \otimes \sum_{i=0}^{2^{2n}-1} |i\rangle .\end{aligned} \tag{20}$$

In the same manner, we must perform the next quantum transformation to assign the color values and coordinates to these sorted positions by the superposed 2^{2n} quantum states from the middle states.

Based on Eqs. (8–10), we can obtain the operator $R^j_{cp,i}$ ($i = 0, 1, \ldots, 2^{2n}-1$; $j = 0, 1, \ldots, 2^k - 1$) by

$$R^j_{cp,i} = \left(I^{\otimes 2} \otimes \left(\sum_{b=0, b\neq i}^{2^{2n}-1} |b\rangle\langle b|\right) \otimes \left(\sum_{d=0, d\neq j}^{2^k-1} |d\rangle\langle d|\right)\right) + R^j_i \otimes |i\rangle\langle i| \otimes |j\rangle\langle j|. \tag{21}$$

In addition, we also have $R^j_{cp,i}\left(R^j_{cp,i}\right)^\dagger = I^{\otimes 2n+k+2}$ ("$\dagger$" denotes the conjugate transpose operator), which means that the quantum transformation operator $R^j_{cp,i}$ is a unitary matrix. Furthermore, we let $R^{(m)}_{cp} = R^0_{cp,0} R^0_{cp,1} \cdots R^0_{cp,2^{2n}-1} R^1_{cp,0} \cdots R^m_{cp,2^{2n}-2} R^m_{cp,2^{2n}-1}$ and apply the quantum transformation operator $R^{(m)}_{cp}$ on $\left|I^{(m)}\right\rangle_{mi}$ gives us the following relation:

$$\begin{aligned}R^{(m)}_{cp}\left(\left|I^{(m)}\right\rangle_{mi}\right) &= R^{(m)}_{cp}\left(\frac{1}{2^{n+\frac{k+1}{2}}} \sum_{j=0}^{2^k-1} |j\rangle \otimes \left(\sum_{l=0}^{1} |l\rangle \otimes |0\rangle\right) \otimes \sum_{i=0}^{2^{2n}-1} |i\rangle\right) \\ &= \frac{1}{2^{k/2}} \sum_{j=0}^{2^k-1} \left(\frac{1}{2^{n+1/2}} \sum_{i=0}^{2^{2n}-1} \left(\cos\theta_{j,i}|00\rangle + \sin\theta_{j,i}|10\rangle + \cos\varphi_{j,i}|01\rangle + \sin\varphi_{j,i}|11\rangle\right) \otimes |i\rangle\right) \otimes |j\rangle \\ &= \frac{1}{2^{n+\frac{k+1}{2}}} \sum_{j=0}^{2^k-1} \sum_{i=0}^{2^{2n}-1} \left(\cos\theta_{j,i}|00\rangle + \sin\theta_{j,i}|10\rangle + \cos\varphi_{j,i}|01\rangle + \sin\varphi_{j,i}|11\rangle\right) \otimes |i\rangle \otimes |j\rangle .\end{aligned} \tag{22}$$

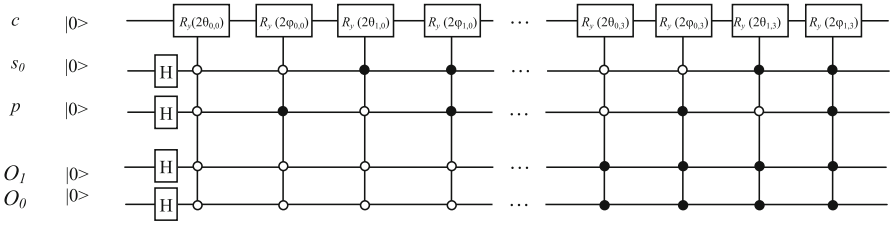

Fig. 7 A simple example of the preparation circuit for the 2OQIM of two quantum images shown in Fig. 6

Fig. 8 0CNOT gate

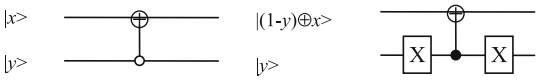

Compared with the OQIM for one single image, the mOQIM for multiple images' preparation take more quantum operations and more quantum gates. We find that the complexity of the preparation of mOQIM is about $O\left(2^{4n+2k}\right)$.

Figure 7 is a simple example of the preparation circuit for the OQIM of two quantum images with $n = 1$, $k = 1$, $m = 2$, in which similarly there are some simple quantum gates such as the Hadamard gate (H gate) and 3-qubit control rotation gate used here to prepare the OQIM.

4.3 mOQIM-based image histogram specification

In this section, we will discuss the mOQIM-based image histogram specification. First, we will discuss the 2OQIM-based image histogram specification (i.e., the image histogram specification for one another between two quantum images). Then we extend the image histogram specification to the multiple images based on the mOQIM.

4.3.1 2OQIM-based image histogram specification

At the beginning, considering the control NOT gate (CNOT), we build the 0-control NOT (0CNOT) ("$\oplus$" denotes "xor") as shown in Fig. 8. In fact, the left 0CNOT can be realized by the right CNOT with two X gates, or to say that the two gates are equivalent.

From Fig. 8, we have

$$0\text{CNOT} = I \otimes |1\rangle\langle 1| + X \otimes |0\rangle\langle 0|, \tag{22}$$

where $X = |1\rangle\langle 0| + |0\rangle\langle 1|$ being the NOT gate.

Now we apply the 0CNOT on the two quantum images as shown in Fig. 7 to obtain Fig. 9. Via Eq. (14), after applying the 0CNOT, we have

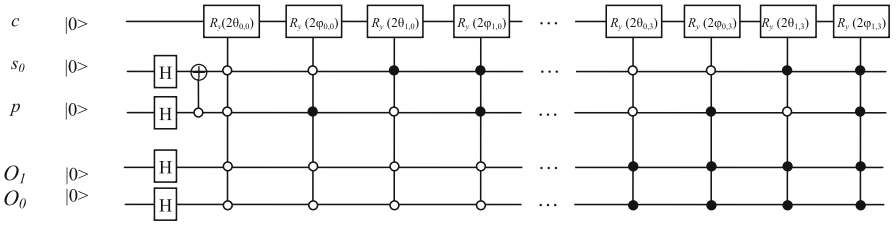

Fig. 9 An example of the histogram specification for one another between two images

$$
\begin{aligned}
I \otimes 0\mathrm{CNOT} \otimes I^{\otimes 2}\left(\left|I^{(2)}\right\rangle\right) &= I \otimes 0\mathrm{CNOT} \otimes I^{\otimes 2}\left(\frac{1}{2^{1/2}}\sum_{j=0}^{1}\left|I_j\right\rangle \otimes |j\rangle\right) \\
&= I \otimes 0\mathrm{CNOT} \otimes I^{\otimes 2}\left(\frac{1}{\sqrt{2}}(|I_0\rangle \otimes |0\rangle + |I_1\rangle \otimes |1\rangle)\right) \\
&= \frac{1}{\sqrt{2}}\left(\left|I_0'\right\rangle \otimes |0\rangle + \left|I_1'\right\rangle \otimes |1\rangle\right), \qquad (23)
\end{aligned}
$$

where

$$
\begin{aligned}
\left|I_1'\right\rangle = \frac{1}{2^{3/2}}\big[&\left(\cos\theta_{0,0}|00\rangle + \sin\theta_{0,0}|10\rangle + \cos\varphi_{1,0}|01\rangle + \sin\varphi_{1,0}|11\rangle\right) \otimes |00\rangle \\
&+ \left(\cos\theta_{0,1}|00\rangle + \sin\theta_{0,1}|10\rangle + \cos\varphi_{1,1}|01\rangle + \sin\varphi_{1,1}|11\rangle\right) \otimes |01\rangle \\
&+ \left(\cos\theta_{0,2}|00\rangle + \sin\theta_{0,2}|10\rangle + \cos\varphi_{1,2}|01\rangle + \sin\varphi_{1,2}|11\rangle\right) \otimes |10\rangle \\
&+ \left(\cos\theta_{0,3}|00\rangle + \sin\theta_{0,3}|10\rangle + \cos\varphi_{1,3}|01\rangle + \sin\varphi_{1,3}|11\rangle\right) \otimes |11\rangle\big],
\end{aligned}
$$

$$
\begin{aligned}
\left|I_0'\right\rangle = \frac{1}{2^{3/2}}\big[&\left(\cos\theta_{1,0}|00\rangle + \sin\theta_{1,0}|10\rangle + \cos\varphi_{0,0}|01\rangle + \sin\varphi_{0,0}|11\rangle\right) \otimes |00\rangle \\
&+ \left(\cos\theta_{1,1}|00\rangle + \sin\theta_{1,1}|10\rangle + \cos\varphi_{0,1}|01\rangle + \sin\varphi_{0,1}|11\rangle\right) \otimes |01\rangle \\
&+ \left(\cos\theta_{1,2}|00\rangle + \sin\theta_{1,2}|10\rangle + \cos\varphi_{0,2}|01\rangle + \sin\varphi_{0,2}|11\rangle\right) \otimes |10\rangle \\
&+ \left(\cos\theta_{1,3}|00\rangle + \sin\theta_{1,3}|10\rangle + \cos\varphi_{0,3}|01\rangle + \sin\varphi_{0,3}|11\rangle\right) \otimes |11\rangle\big].
\end{aligned}
$$

Clearly, through Eq. (23) (performing the histogram specification via the circuit shown in Fig. 9), we obtain the histogram specification for one another between the two images $|I_0\rangle, |I_1\rangle$. Finally, the histogram specification images are $\left|I_1'\right\rangle$ and $\left|I_0'\right\rangle$ (equivalent to the exchanging of the histograms between the two images). We also find that the complexity of the histogram specification for the two images is only $O(1)$, that is much faster than the traditional histogram specification in the classical computer whose histogram specification's complexity is about $O\left(2^{2n}\right)$ because of assigning every pixel. This comparison indicates the quantum computer's great advantage over the traditional one in parallel computation.

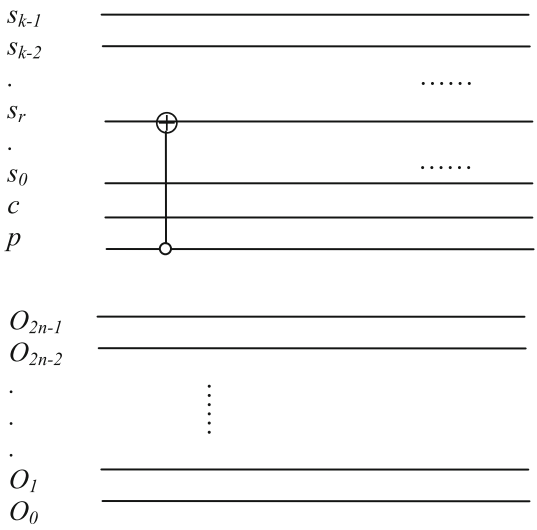

Fig. 10 The circuit of histogram specification for multiple images based on mOQIM ($r=0,1,\ldots,k-1$)

4.3.2 mOQIM-based parallel multiple image histogram specification

Similar with the case of $m = 2$, when $m > 2$, we can perform the multiple image histogram specification in the similar manner by applying 0CNOT gate on different line $s_r (r = 0, 1, \ldots, k-1)$. However, the difference is also very obvious. For example, if we apply 0CNOT gate on the line $s_r (r = 0, 1, \ldots, k-1)$ as shown in Fig. 10, we can obtain the parallel multiple image histogram specification between the images encoded by $|s_{k-1}s_{k-2}\cdots s_{r+1}0s_{r-1}\cdots s_1 s_0\rangle$ and $|s_{k-1}s_{k-2}\cdots s_{r+1}1s_{r-1}\cdots s_1 s_0\rangle$, respectively ($s_{l=0,1,\cdots,k-1} \in \mathrm{B}$). That is to say, only applying the 0CNOT gate on one single line s_r, we can obtain the parallel multiple image histogram specification synchronously for $2 \times 2^{k-1} = 2^k$ images.

We set $U_r = I^{\otimes 2n+k} \otimes 0CNOT$, then

$$U_r\left(\left|I^{(m)}\right\rangle\right) = U_r\left|I^{(m)}\right\rangle = \frac{1}{2^{k/2}}\sum_{j=0}^{2^k-1} U_r\left(|I_j\rangle \otimes |j\rangle\right) = \frac{1}{2^{k/2}}\sum_{j=0}^{2^k-1}\left|I'_j\right\rangle \otimes |j\rangle, \tag{24}$$

where $\left|I'_j\right\rangle = \frac{1}{2^{n+1/2}}\sum_{i=0}^{2^{2n}-1}\left(\cos\theta_{j',i}|00\rangle + \sin\theta_{j',i}|10\rangle + \cos\varphi_{j,i}|01\rangle + \sin\varphi_{j,i}|11\rangle\right)\otimes|i\rangle$ and $\left|j'-j\right| = 2^r$.

Clearly, only, respectively, applying the 0CNOT gate on the lines s_r ($r \in \{0, 1, \ldots, k-1\}$), we can obtain multiple image histogram specification for 2^k images. Therefore, the histogram specification's complexity of our method is $O(1)$. Contrastively, for the same results of the histogram specification as ours, in the classical computer it needs much more times' operations, and the histogram specification's complexity in traditional image processing is about $O\left(2^{2n+k}\right)$, which is much more

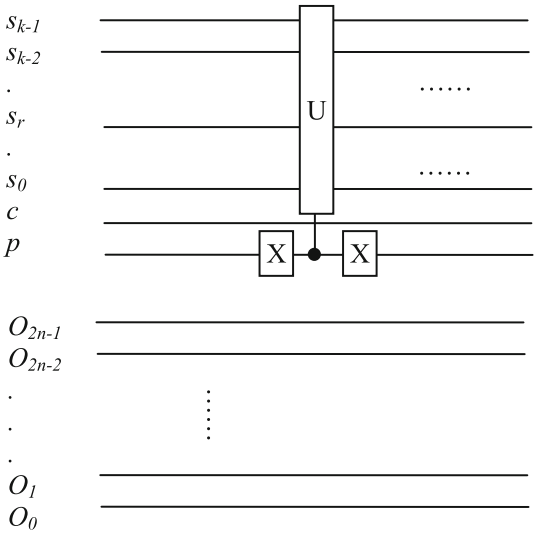

Fig. 11 The circuit of histogram specification for any image pair based on mOQIM ($r=0,1,\ldots,k-1$)

than the complexity $O(1)$ of our method. This comparison shows the great advantage of our mOQIM in histogram specification.

Figure 10 is the circuit of histogram specification for multiple images based on mOQIM, in which we can perform 0CNOT operation on s_r to obtain the parallel multiple image histogram specification for 2^k images based on the mOQIM.

4.3.3 mOQIM-based any histogram specification for multiple images

In the above section, we have shown the mOQIM-based parallel multiple image histogram specification with the advantages over the classical methods. However, here we only can perform the histogram specification between the images $|I_{j_1}\rangle$ and $|I_{j_2}\rangle$ (with $|j_1 - j_2| = 2^r$) for a fixed r. For example, when $k = 2$ and $r = 0$, we exchange the histograms between the image pairs: $|I_0\rangle$ and $|I_1\rangle$, $|I_2\rangle$ and $|I_3\rangle$. If $k = 2$ and $r = 1$, we exchange the histograms between the image pairs: $|I_0\rangle$ and $|I_2\rangle$, $|I_1\rangle$ and $|I_3\rangle$. We find that it is impossible by only applying one time's 0CNOT gate on the line $s_r(s_0$ or $s_1)$ to exchange the histograms between the image pairs ($|I_0\rangle$ and $|I_3\rangle$, or $|I_1\rangle$ and $|I_2\rangle$). Therefore, we have to apply two 0CNOT gates on the line s_0 and s_1, respectively, at the same time to exchange the histograms between the image pairs ($|I_0\rangle$ and $|I_3\rangle$, $|I_1\rangle$ and $|I_2\rangle$). Then how to exchange the histograms (perform the histogram specification) between the images $|I_{j_1}\rangle$ and $|I_{j_2}\rangle$ (with $|j_1 - j_2| \neq 2^r$ and $r \in \{0, 1, \ldots, k-1\}$)? The answer is to apply multiple 0CNOT gates at the same time via more control conditions. See Fig. 11 for the circuit of histogram specification for any image pair based on mOQIM.

For example, if we want to perform the histogram specification between the two images ($|I_{34}\rangle$,$|I_{38}\rangle$) from one another (see Fig. 12), we can build the 6-control not gate (6CNOT), and the control bits are $|s_5 s_4 s_3 s_1 s_0 p\rangle = |100100\rangle$, the controlled bit is $|s_2\rangle$.

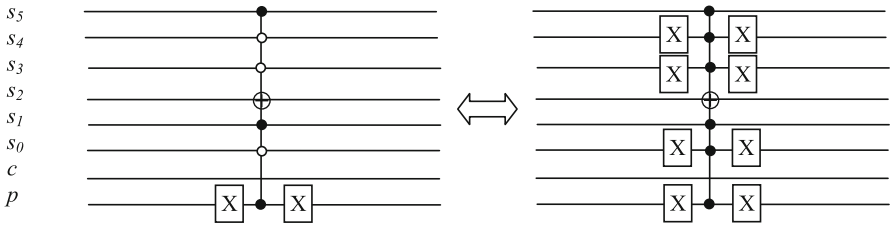

Fig. 12 The circuit of histogram specification between the image pair ($|I_{34}\rangle$,$|I_{38}\rangle$) based on mOQIM ($k=6$)

In Fig. 12, we have

$$U = \Big(I \otimes X^{\otimes 2} \otimes I^{\otimes 2} \otimes X \otimes I \otimes X\Big)(C(U_2))\Big(I \otimes X^{\otimes 2} \otimes I^{\otimes 2} \otimes X \otimes I \otimes X\Big),$$

where $C(U_2)$ is the controlled U gate which is shown in the right (the middle) of Fig. 12.

Thus via this way we can perform any histogram specification between any image pair ($\left|I_{j_1}\right\rangle$ and $\left|I_{j_2}\right\rangle$, with $j_1 \neq j_2$ and $j_1, j_2 \in \{0, 1, \ldots, m-1\}$).

On the other hand, we can design the histogram with any wanted shape and perform parallel histogram specification for multiple images. How to perform parallel histogram specification for multiple images at the same time?

Theorem 1 *For $m = 2^k$ classical image $f_j(x, y)(j = 1, 3, 5, \ldots, 2^{k+1}-3, 2^{k+1}-1)$ and the given image $f(x, y)$ with any wanted histogram, we set $f_j(x, y) \equiv f(x, y)$ $(j = 0, 2, 4, \ldots, 2^{k+1}-4, 2^{k+1}-2)$, their order-encoded quantum image model (called as (m + 1)OQIM) is defined as follows:*

$$\left|I^{(m+1)}\right\rangle = \frac{1}{2^{(k+1)/2}} \sum_{j=0}^{2^{k+1}-1} \left|I_j\right\rangle \otimes |j\rangle, \tag{25}$$

where

$$|j\rangle = |s_k s_{k-1} s_{k-2} \cdots s_1 s_0\rangle = \left\{ \left| \underbrace{00\cdots00}_{k+1} \right\rangle, \left| \underbrace{00\cdots01}_{k+1} \right\rangle, \cdots, \left| \underbrace{11\cdots11}_{k+1} \right\rangle \right\},$$

$$\left|I_j\right\rangle = \frac{1}{2^{n+1/2}} \sum_{i=0}^{2^{2n}-1} \left(\cos\theta_{j,i}|00\rangle + \sin\theta_{j,i}|10\rangle + \cos\varphi_{j,i}|01\rangle + \sin\varphi_{j,i}|11\rangle\right) \otimes |i\rangle$$

if j is odd,

$$\left|I_j\right\rangle = \frac{1}{2^{n+1/2}} \sum_{i=0}^{2^{2n}-1} (\cos\theta_i|00\rangle + \sin\theta_i|10\rangle + \cos\varphi_i|01\rangle + \sin\varphi_i|11\rangle) \otimes |i\rangle \text{ if}$$

j is even(θ_i, φ_i are mapped from $f(x, y)$);

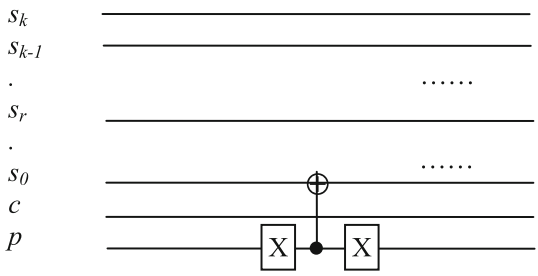

Fig. 13 The circuit of parallel histogram specification for multiple images with any wanted histogram of the designed $f(x, y)$

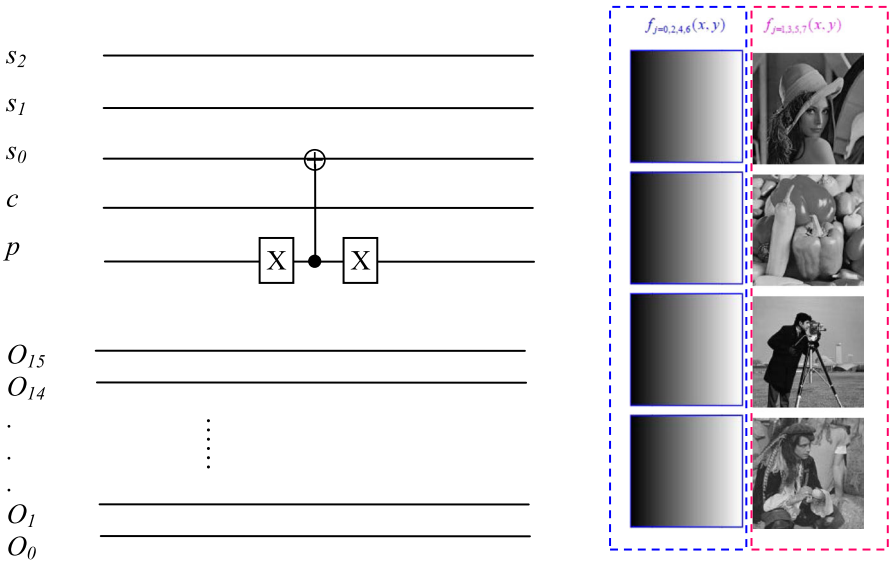

Fig. 14 The circuit of an experiment to perform the parallel histogram specification for four images with our wanted histogram of the designed $f(x, y)$

and now we can apply the 0CNOT gate on the line s_0 via p line controlling to perform the parallel histogram specification for multiple images with the any wanted histogram from the given designed $f(x, y)$.

The proof of Theorem 1 is trivial by the above sections in this paper and can be obtained very easily. Figure 13 shows the procedure of Theorem 1 for the circuit of parallel histogram specification for multiple images with any wanted histogram of the designed $f(x, y)$.

Thus, we know that the preparation of the $(m + 1)$OQIM needs $2n + k + 3$ qubits. We find that the complexity of the preparation of $(m + 1)$OQIM is also about $O\left(2^{4n+2k}\right)$ because of the even positions' same image.

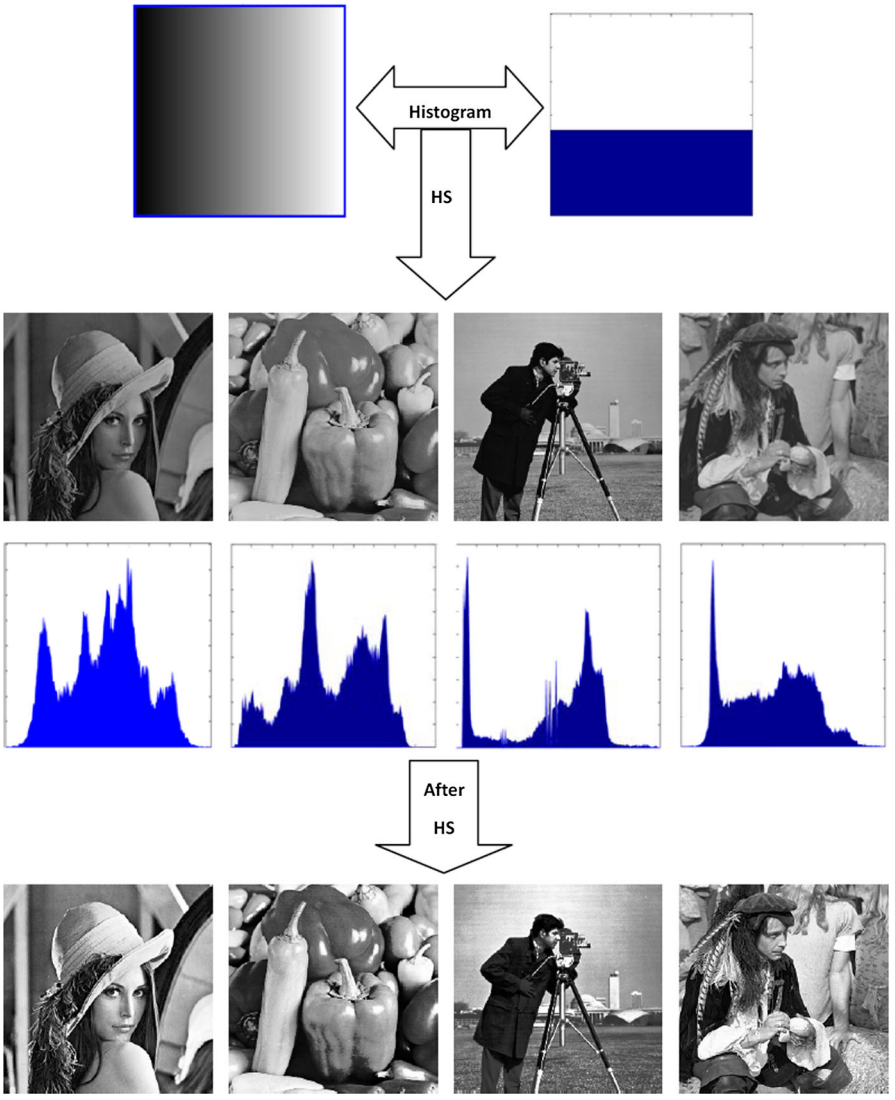

Fig. 15 The simulative experiment of the parallel histogram specification for four images with the designed equalized histogram from the designed $f(x, y)$

On the other hand, the histogram specification's complexity in Theorem 1 is $O(1)$(i.e., only one time's operation on line s_0). Contrastively, for the same results of the histogram specification as ours, in the classical computer it needs much more times' operations with the complexity of $O\left(2^{2n+k}\right)$ via assigning every pixel's value, which is much more than the complexity $O(1)$ of our method. This comparison shows the great advantage of our (m + 1)OQIM in histogram specification.

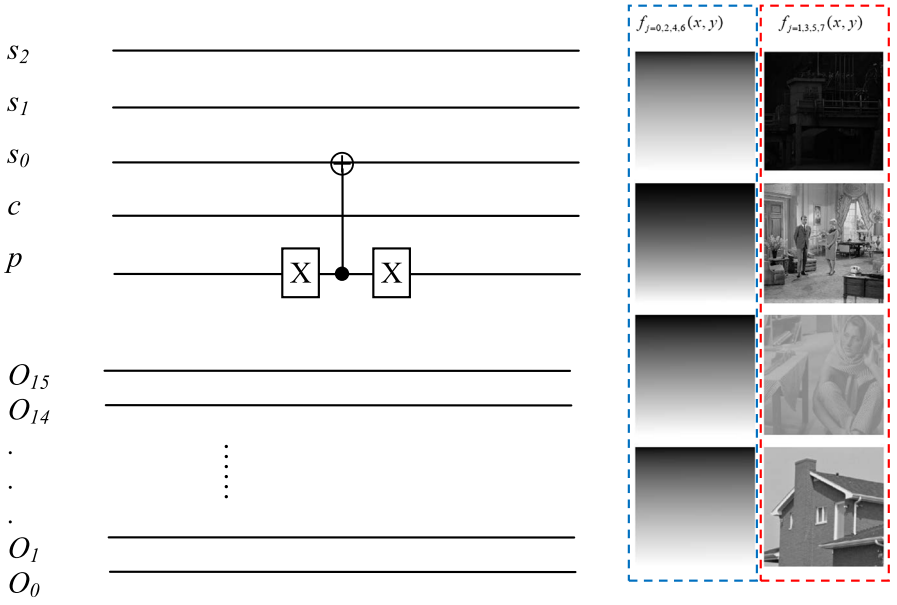

Fig. 16 The circuit of an experiment to perform the parallel image enhancement by histogram specification for four images with our wanted histograms of the four designed images

5 Experiments

5.1 Parallel histogram specification

In this section, we design an experiment to perform the parallel histogram specification for multiple images with our designed histogram in the designed $f(x, y)$. The designed image $f(x, y)$ enclosed by blue-line squares has the equalized histogram shown in Fig. 14 (i.e., $f_{j=0,2,4,6}(x, y) \equiv f(x, y)$). The four images ($f_{j=1,3,5,7}(x, y)$) on which the histogram specification will be applied are shown in the right of Fig. 14 as well. All the images have the size 256×256 and gray values (8-bit: 0–255). Of course, we also can design the given image $f(x, y)$ with other wanted histogram of different shape if necessary.

The results can be seen in Fig. 15. We find that the histogram specification's complexity in this experiment is $O(1)$(i.e., only one time's operation/0CNOT on line s_0). Contrastively, for the same results of the histogram specification, in the classical computer it needs much more times' operations about the complexity of $O\left(2^{20}\right)$ via assigning every pixel's value, which is much more than the complexity $O(1)$ of our method. This experiment shows the great advantage of our $(m + 1)$OQIM in histogram specification.

As shown in Figs. 14, 15, we only showed an experiment of the parallel histogram specification for four images with the designed equalized histogram from the designed $f(x, y)$. In addition, since the designed $f(x, y)$ has the equalized histogram, we indeed performed the parallel histogram equalization for the four images at one time.

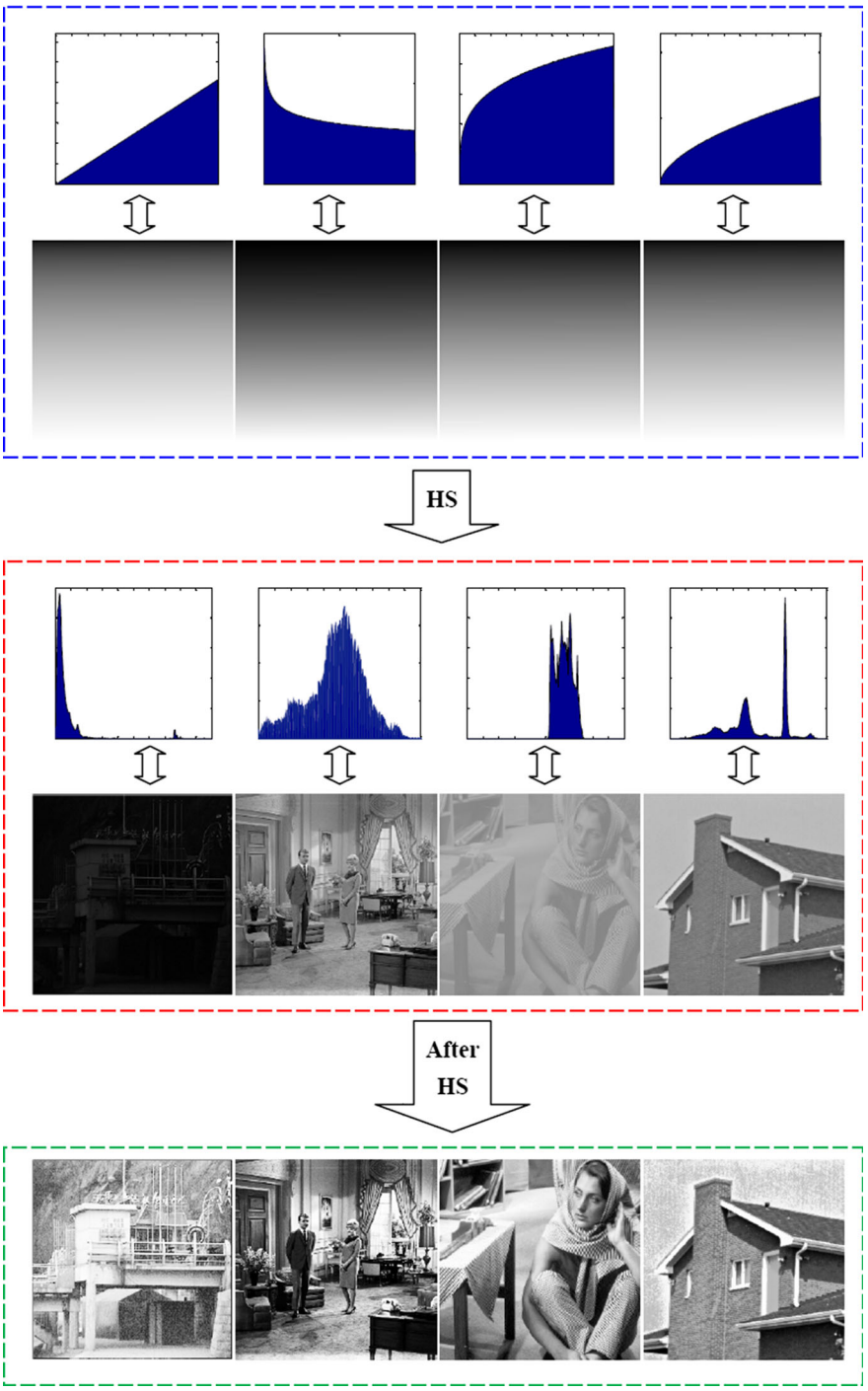

Fig. 17 The simulative experiment of the parallel image enhancement by histogram specification for four images with the designed equalized histograms from the designed $f(x, y)s$

Table 1 The complexity comparison between our methods and the classical counterparts

	Complexity			
	Related to the size $2^n \times 2^n$ of images		Related to number m of images	
	Our method	Classical method	Our method	Classical method
Histogram specification	$O(1)$	$O\left(2^{2n}\right)$	$O(1)$	$O(m)$
Image enhancement	$O(1)$	$O\left(2^{2n}\right)$	$O(1)$	$O(m)$

5.2 Parallel quantum image brightness enhancement

Different from the previous experiment shown in 5.1, in this section we will show an experiment to perform the parallel image enhancement for multiple images with our designed histograms in the multiple different designed $f(x, y)s$ at the same time. The designed images $f(x, y)s$ enclosed by blue-line squares have the different histograms encoded for the further enhancement. Similarly, the four images enclosed by red-line squares are the images to be enhanced shown in Fig. 16.

The four images $(f_{j=1,3,5,7}(x, y))$ on which the histogram specification will be applied are shown in the right of Fig. 16 as well. All the images have the size 256×256 and gray values (8-bit: 0–255). The results can be seen in Fig. 17. We find that the image enhancement's complexity in this experiment is $O(1)$ (i.e., only one time's operation/0CNOT on line s_0). Contrastively, for the same results of the image enhancement, in the classical computer it needs much more times' operations about the complexity of $O\left(2^{20}\right)$ via assigning every pixel's value, which is much more than the complexity $O(1)$ of our method. This experiment shows the great advantage of our $(m + 1)$OQIM in histogram specification. That is to say, our methods obtain the exponential speedup. In other words, the newly proposed method can complete the parallel histogram specification via only one single quantum operation, i.e., the complexity is free of the image size and the number of the images to be processed. The complexity comparison between our proposed methods and the classical counterparts can be found in Table 1.

Similarly, if the designed $f(x, y)$ has other different histogram, we can perform different histogram specification such as luminance correction and so on to realize image enhancement.

6 Conclusions and future work

Compared with the existing quantum image representation models, the OQIM/mOQIM has the following features:

(1) The newly proposed quantum image representation OQIM/mOQIM uses the basis state of a qubit sequence to store the ascending order of each pixel according to their gray values' magnitude for the first time to our best knowledge;

(2) The OQIM/mOQIM uses the amplitude probability of a qubit to store the color and uses the amplitude probability of another qubit to store the coordinate position of each pixel at the same time;
(3) The OQIM/mOQIM can effectively encode the information of the histograms of the images; thus, the histogram specification of two images and even the parallel histogram specification at the same time for multiple images can be easily performed with much less computation complexity than the classical counterpart. In other words, the newly proposed method can complete the parallel histogram specification via only one single quantum operation, i.e., the complexity is free of the image size and the number of the images to be processed.

Finally, experiments and theoretical analysis show that the proposed OQIM/mOQIM quantum image model is more flexible and better suited for the histogram specification in parallel including histogram equalization and other similar image enhancement method such as luminance correction and so on than the existing quantum image models.

Our future work includes the other image processing tasks such as image comparison and image searching, image filtering and image completion and so on [5, 27, 28] based on the proposed OQIM/mOQIM quantum image model. In addition, we will perform our experiments on the quantum simulation systems in future.

Acknowledgements This work is fully supported by NSFCs (6197050275, 61471412, 61771020) and LZ15F020001.

References

1. Feynman, R.P.: Simulating physics with computers. Int. J. Theor. Phys. **21**(6/7), 467–488 (1982)
2. Shor, P.W.: Algorithms for quantum computation: discrete logarithms and factoring. In: Proceedings of the 35th Annual Symposium on Foundations of Computer Science. IEEE Computer Soc. Press, Los Almitos, CA, pp. 124–134 (1994)
3. Grover, L.: A fast quantum mechanical algorithm for database search. In: Proceedings, 28th Annual ACM Symposium on the Theory of Computing (STOC 1996). ACM, New York, pp. 212–219 (1996)
4. Nielsen, M., Chuang, I.: Quantum Computation and Quantum Information. Cambridge University Press, New York (2000)
5. Gonzalez, R.C., Woods, R.E.: Digital Image Processing, 3rd edn. Prentice Hall, Upper Saddle River (2007)
6. Le, P.Q., Dong, F., Hirota, K.: A flexible representation of quantum images for polynomial preparation, image compression and processing operations. Quantum Inf. Process. **10**(1), 63–84 (2010)
7. Venegas-Andraca, S.E., Bose, S.: Storing, processing and retrieving an image using quantum mechanics. Proc. SPIE Conf. Quantum Inf. Comput. **5105**, 137–147 (2003)
8. Sun, B., Le, P.Q., Iliyasu, A.M.: A multi-channel representation for images on qunatum computers using the *RGBα* color space. In: IEEE 7th International Symposium on Intelligent Signal Processing, Floriana, Malta, 2011, pp. 1–6 (2011)
9. Li, H.S., Zhu, Q.X., Zhou, R.G., Li, M.C., et al.: Multidimensional color image storage, retrieval, and compression based on qunatum amplitudes and phases. Inf. Sci. **273**, 212–232 (2014)
10. Zhang, Y., Lu, K., Gao, Y.H., Xu, K.: A novel quantum representation for log-polar images. Quantum Inf. Process. **12**(9), 3103–3126 (2013)
11. Zhang, Y., Lu, K., Gao, Y.H., Wang, M.: NEQR: a novel enhanced quantum representation of digital images. Quantum Inf. Process. **12**(8), 3340–3343 (2013)
12. Sang, J., Wang, S., Li, Q.: A novel quantum representation of color digital images. Quantum Inf. Process. **16**(42), 1–14 (2017)

13. Yuan, S., Mao, X., Xue, Y., Chen, L., Xiong, Q., Compare, A.: SQR: a simple quantum representation of infrared images. Quantum Inf. Process. **13**, 1353–1379 (2014)
14. Li, H.-S., Qingxin, Z., Lan, S., Shen, C.-Y., Zhou, R., Mo, J.: Image storage, retrieval, compression and segmentation in a quantum system. Quantum Inf. Process. **12**, 2269–2290 (2013)
15. Venegas-Andraca, S.E., Ball, J.L., Burnett, K., Bose, S.: Processing images in entangled quantum systems. Quantum Inf. Process. **9**, 1–11 (2010)
16. Latorre, J.I.: Image compression and entanglement (2005). arXiv:quant-ph/0510031
17. Jiang, N., Wang, L.: Quantum image scaling using nearest neighbor interpolation. Quantum Inf. Process. **14**(5), 1559–1571 (2015)
18. Jiang, N., Wang, J., Mu, Y.: Quantum image scaling up based on nearest-neighbor interpolation with integer scaling ratio. Quantum Inf. Process. **14**(11), 4001–4026 (2015)
19. Jiang, N., Dang, Y.J., Wang, J.: Quantum image matching. Quantum Inf. Process. **15**(9), 3543–3572 (2016)
20. Jiang, N., Dang, Y.J., Zhao, N.: Quantum image location. Int. J. Theor. Phys. **55**(10), 4501–4512 (2016)
21. Coltuc, D., Bolon, P., Chassery, J.-M.: Exact histogram specification. IEEE Trans. Image Process. **15**(5), 1143–1152 (2006)
22. Sun, C.-C., Ruan, S.-J., Shie, M.-C., Pai, T.-W.: Dnamic contrast enhancement based on histogram specification. IEEE Trans. Consum Electron **51**(4), 1300–1305 (2005)
23. Weiss, Y., Elovici, Y., Rokach, L.: The CASH algorithm-cost-sensitive attribute selection using histograms. Inf. Sci. **222**, 247–268 (2013)
24. Stark, J.A.: Adaptive image contrast enhancement using generalizations of histogram equalization. IEEE Trans. Image Process. **9**(5), 889–896 (2000)
25. Villegas, M., Paredes, R.: Comparison of illumination normalization methods for face recognition. In: Third COST 275 Workshop, pp. 27–30 (2005)
26. Shan, S., Gao, W., Cao, B., Zhao, D.: Illumination normalization for robust face recognition against varying lighting conditions. In: Proceedings of the AMFG (2003)
27. Scabini, L.F., Condori, R.H., Gonçalves, W.M., Brunoa, O.M.: Multilayer complex network descriptors for color–texture characterization. Inf. Sci. **491**, 30–47 (2019)
28. ThanhNguyen, T., TruongDang, M., WeeChungLiew, A., Bezdek, J.C.: A weighted multiple classifier framework based on random projection. Inf. Sci. **490**, 36–58 (2019)
29. Hai-Sheng, L., Ping, F., Hai-Ying, X., et al.: Quantum implementation circuits of quantum signal representation and type conversion. IEEE Trans. Circuits Syst. I: Regul. Pap. **2018**, 1–14 (2018)
30. Li, H.S., Chen, X., Xia, H.Y., et al.: A quantum image representation based on bitplanes. IEEE Access **2018**, 1–1 (2018)
31. Jiang, N., Dong, X., Hu, H., et al.: Quantum image encryption based on Henon mapping. Int. J. Theor. Phys. **58**(3), 979–991 (2019)
32. Zhang, T.C., Zhang, J., Zhang, J.P., et al.: Review of methods of image segmentation based on quantum mechanics. J. Electron. Sci. Technol. **16**(3), 53–62 (2018)
33. Li, H.S., Zhu, Q., Zhou, R.G., et al.: Multi-dimensional color image storage and retrieval for a normal arbitrary quantum superposition state. Quantum Inf. Process. **13**(4), 991–1011 (2014)